



Chitosan dual gel-like functionalized with flavonoid extract and cinnamaldehyde oil using dual cross-linking agents: Characterization, antioxidant, and antimicrobial effects

Mahmoud Salah^{a,b}, Juanying Huang^a, Chenyang Zhu^a, Mabrouk Sobhy^c, Mohamed A. Farag^d, Yajing Fang^{e,f}, Remah Sobhy^g, Noman Walayat^h, Ibrahim Khalifa^{a,i,j,**}, Sajid Maqsood^{j,*}, Yun Wang^{a,***}

^a Laboratory of prevention and detection of microbial and chemical contamination in foods, School of Food and Biological Engineering, Jiangsu University, Zhenjiang, 212013, China

^b Department of Environmental Agricultural Science, Faculty of Graduate Studies and Environmental Research, Ain Shams University, Cairo, 11566, Egypt

^c Food Science and Technology Department, Faculty of Agriculture, Alexandria University, 21545, El-Shatby, Alexandria, Egypt

^d Pharmacognosy Department, College of Pharmacy, Cairo University, Cairo, P.B. 11562, Egypt

^e School of Food Science and Engineering, Key Laboratory of Food Nutrition and Functional Food of Hainan Province, Hainan University, Haikou, 570228, China

^f Collaborative Innovation Center of One Health, Hainan University, Haikou, 570228, China

^g Department of Biochemistry, Faculty of Agriculture, Benha University, 13736, Moshtohor, Qalubia, Egypt

^h College of Tea Science and Tea Culture, Zhejiang Agriculture and Forestry University, Hangzhou, 311300, China

ⁱ Food Technology Department, Faculty of Agriculture, Benha University, 13736, Moshtohor, Qalubia, Egypt

^j Department of Food Science, College of Agriculture and Veterinary Medicine, United Arab Emirates University, Al-Ain, 15551, United Arab Emirates

ARTICLE INFO

Keywords:

Orange peel extract
Ionic gelation
Essential oils
Antimicrobial properties
Chitosan gel

ABSTRACT

This study evaluated antioxidant and antimicrobial properties of chitosan gel (Cs-gel) functionalized with cinnamaldehyde oil (CN) and orange peel-derived flavonoid extract (Fs) using the ionic-gelation method. Results showed that the encapsulation efficiencies of CCF-9 and CCN were 83.14 ± 3.34 and $80.56 \pm 1.17\%$, respectively. The interaction of CN or Fs on Cs-gel indicates the presence of H-bonding formation, as observed by UV-vis spectroscopy, Fourier transform infrared spectrophotometry (FTIR), and Raman-spectroscopy showed a good corroboration with Surfex-dock findings. Scanning electron microscopy also showed the integration that occurred between Cs and both ligands, which was further supported with X-ray diffraction and X-Ray photoelectron spectroscopy spectra. The textural properties of CCF-5 gel showed high hardness, chewiness, and gumminess values, indicating that the integration of Fs and CN altered the microstructure of Cs-gel. Chitosan-functionalized based gels exhibited higher antioxidant abilities against DPPH and ABTS free radicals than Cs-gel. The CCF-9 gel showed a good inhibition value of 29.91 ± 1.22 and $93.61 \pm 2.12\%$ against *Penicillium expansum* and *Alternaria westerdijkiae*, respectively. Additionally, CCF-9 inhibition zones against *Staphylococcus aureus*, *Escherichia coli*, and *Bacillus cerues* were 28.65 ± 0.05 , 27.69 ± 0.04 , and 26.16 ± 0.02 mm, respectively. These findings demonstrated the potential antioxidant and antimicrobial effects of functionalized chitosan gel indicating its potential as a bioactive additive for food preservation.

1. Introduction

Food products are liable to spoilage before and even after processing,

causing major economic losses for producers (Hernández et al., 2021). Alongside chemical and physical contamination, microbes are mainly responsible for food spoilage that is caused by growth of mold and/or

* Corresponding author.

** Corresponding author. Laboratory of prevention and detection of microbial and chemical contamination in foods, School of Food and Biological Engineering, Jiangsu University, Zhenjiang, 212013, China.

*** Corresponding author.

E-mail addresses: ibrahim.khalifa@fagr.bu.edu.eg (I. Khalifa), sajid.m@uaeu.ac.ae (S. Maqsood), wangy1974@ujls.edu.cn (Y. Wang).

<https://doi.org/10.1016/j.crf.2024.100826>

Received 6 June 2024; Received in revised form 12 August 2024; Accepted 19 August 2024

Available online 23 August 2024

2665-9271/© 2024 The Authors. Published by Elsevier B.V. This is an open access article under the CC BY-NC license (<http://creativecommons.org/licenses/by-nc/4.0/>).

bacteria, *i.e.*, *Penicillium expansum*, *Aspergillus flavus*, *Escherichia coli*, *Staphylococcus aureus*, and *Bacillus subtilis* through inefficient temporary-storage and packaging operations (Garcia et al., 2019). Therefore, synthetic chemicals are the main approach used to control the post-harvest microbial contamination in fruits and vegetables (Gong et al., 2024; Tu et al., 2024). In addition to the toxicity of these synthetic additives and their direct or indirect delivery to humans that can lead to different health concerns, thus demanding to explore effective methods, eco-friendly strategies, and efficient additive alternatives to mitigate the food contamination.

In this context, phytochemicals and volatiles have been spotlighted as natural anti-spoilage agents (Lai et al., 2024). For instance, essential oils and flavonoids that contain hydrophobic groups and can show antimicrobial activity through binding with the phospholipids of the cell membranes, were recommended. Flavonoids (Fs) produced naturally in citrus fruits have shown antioxidants, antibacterial properties, and compatibility with probiotics (Addi et al., 2021). For instance, Fs which was abundantly found in Navel orange peels showed antibacterial properties and preservation effects (Zhang et al., 2022). These properties could be enhanced via synergistically conjugating with essential oils for wide-range applications, meanwhile the underlying mechanism of the functionality of Fs depends on their structure, hydroxylation level, substitution, conjugation, and polymerization degree (Thebti et al., 2023). For example, cinnamaldehyde (CN) which is a bioactive essential oil extracted from cinnamon could act as a flavor-enhancing and antimicrobial food additive (Guo et al., 2022; Predoi et al., 2018). It inhibits the growth of *S. aureus* (Gram-positive), *E. coli*, and *Salmonella* spp. (Gram-negative) bacteria (Doyle and Stephens., 2019) via cell membrane degradation and ATPase activity inhibition. Meanwhile, CN and Fs have some disadvantages, namely weak thermal stability, low water solubility, and a high oxidation rate in oxygen-rich environments (Li et al., 2018; Subhaswaraj et al., 2018). Thus, overcoming their limitations and amending their stability using conjugation and/or encapsulation are needed.

Gel developed from polysaccharides via ionic gelation by cross-linkers is one of the outstanding approaches to enhance the bioactive components' stability. It has a great potential for nanomaterial applications, *i.e.*, antimicrobial properties and drug delivery (Adame et al., 2024; Pereira Silveira, Lucas Chaves Almeida, Dutra Alvim and Silvia Prata, 2023). Chitosan gel (Cs) is a delivery system that fully delivers phytochemicals and controls their releasing rate (Do et al., 2022). Cs has been utilized in various fields, such as controlling post-harvest diseases in agricultural products caused by pathogens, owing to its nontoxicity, biodegradability, and biocompatibility properties (Coutinho et al., 2020; Ren et al., 2021). Cs is a cationic polymer that helps bind with the negative charge molecules at the cell surface, affecting plasma membrane permeability, and leading to cell death. Meanwhile, modification of the polymer chain's functional groups and/or admixing among phytochemicals can improve its performance and reduce the required doses of microbicides (Ding et al., 2021; Predoi et al., 2023).

We hypothesized that encapsulating CN and Fs using gelation method might enhance their antimicrobial effects. Thus, we aimed at fabricating Cs-gel functionalized with CN and Fs using dual cross-linkers. The physicochemical properties of CN and Fs encapsulated into Cs-gel were evaluated via UV-vis spectroscopy, Fourier transform infrared spectroscopy (FTIR), X-ray diffraction (XRD), X-ray photoelectron spectroscopy (XPS), Raman spectroscopy, and scanning electron microscope (SEM), and further their *in-vitro* DPPH and ABTS antioxidant capacities. The *in-vitro* antimicrobial effects against *P. expansum*, *A. westerdijkiae*, *S. aureus*, *E. coli*, and *B. cereus* were also evaluated. The texture properties and releasing profiles of gels were investigated.

2. Materials and methods

2.1. Materials

Chitosan (Cs) with a minimum purity of 85% and a deacetylation degree of 95.0% was acquired from Zhejiang Golden-Shell Pharmaceutical Co., Ltd., located in China. 2,2-Azino-bis-(3 ethylbenzothiazoline-6-sulfonic acid) the 2-ammonium salt (ABTS), 2,2-diphenyl-1-picrylhydrazyl (DPPH), and cinnamaldehyde oil (with a purity greater than 98% and a molecular weight of 132.16) were purchased from Shanghai Macklin Biochemical Co., Ltd. in Shanghai, China. Orange fruits were acquired from a nearby grocery in Zhenjiang City, Jiangsu, China. Additional compounds have the quality of analytical grade.

2.2. Extraction and purification of flavonoids from orange waste

In summary, a 10 g of orange peel samples were subjected to extraction using 100 mL of 100% EtOH (1:10 w/v) at a temperature of 37 °C. It was then stirred using a magnetic stirring for 6 h at a speed of 200 RPM following the method of Salah and Xu (2021). The extracts were subsequently filtered through a Whatman No. 2 filter paper to eliminate peel particles, and the resulting residue was re-extracted using the same procedure. The extract was subjected into an AB-8 macroporous resin column, and the purified extract was separated using EtOH (80%). The flavonoid extract was concentrated using rotary evaporator until the volume reached 5 mL. To assess the purification process, HPLC-Shimadzu LC-20AT-UVD equipped with a Shimadzu packed column (VP-ODS) was used. The mobile phase used for separation was a mixture of acetonitrile (A) and H₂O (B) with a gradient elution. The proportions of A and B varied over time as follows: 10–25% A from 0 to 15 min, 25–35% A from 15 to 25 min, 35–50% A from 25 to 50 min, 50–90% A from 50 to 60 min, 90% A from 60 to 70 min, and 90-10% A from 70 to 75 min. The injection volume was 20 µL, with a flow rate of 1.0 mL/min, at a temperature of 20 °C. The detection wavelength was set at 285 nm as shown Fig. S1.

2.3. Total flavonoid contents in purified orange extract

100 µL of orange peel extract (5 mg/mL) was mixed with 20 µL of 10% AlCl₃, 300 µL of EtOH, and 20 µL of 1M sodium acetate. Then, the suspension was equilibrated for 30 min at 25 °C in the dark place, and the UV absorption was recorded at a wavelength of 415 nm. Finally, the rutin equivalent (mg/g dry flavonoid extract) was used as a standard curve.

2.4. Preparation of cinnamaldehyde oil (CN) loaded on chitosan gel (Cs-gel) using tripolyphosphate (TPP)

The ionic-gelation method was used to encapsulate CN within the Cs-gel using tripolyphosphate (TPP) as a cross-linker agent according to Ding et al. (2021). Chitosan, at a concentration of 5 mg/mL, was dispersed in a solution of 1% (v/v) acetic acid with a pH of 4.8. Then, CN, at a concentration of 250 µg/mL, was added to the mixture and agitated for 90 min in a dark environment. Afterward, a solution of TPP with a concentration of 5 mg/mL was gradually added in a ratio of 2:1 (v/v). The mixture was then stirred at room temperature for 90 min and centrifuged at a speed of 9660×g for 40 min. Subsequently, the precipitated gel (termed as CCN) was dissolved in 1% (v/v) acetic acid with a pH 4.7 and kept at 4 °C.

2.5. Preparation of flavonoid extract (Fs) loaded on CCN using phytic acid (Pa)

Different concentrations of Fs were loaded on CCN gel using the ionic-gelation method with the aid of phytic acid as a cross-linker agent. Briefly, CCN (5 mg/mL) was dispersed in a solution of 1% (v/v) acetic

acid with a pH of 4.8, and the concentration of Fs (3 mg/mL, CCF-3), (5 mg/mL, CCF-5), (7 mg/mL, CCF-7) and (9 mg/mL, CCF-9) was added to CCN solution then agitated for 90 min in a dark environment. Afterward, 5 mg/mL of Pa was added dropwisely at a flow rate of 1 mL/min and stirred for 90 min. The suspension reaction was centrifuged at 9660×g for 40 min, and the gel was then dispersed in a solution of 1% (v/v) acetic acid and kept at 4 °C.

2.6. Entrapment efficiency (EE %)

The EE of Cs-gel for CN and Fs was determined as reported by Arya et al. (2022). After the centrifugation step, the free CN and Fs in the supernatants were determined using UV-vis spectroscopy at a wavelength of 287 and 280 nm, respectively. The following equations were used to calculate the EE (%):

$$EE (\%) = \frac{CN \text{ initial content} - \text{Free} - CN \text{ in the supernatants}}{CN \text{ initial content}} \times 100 \quad (1)$$

$$EE (\%) = \frac{Fs \text{ initial content} - \text{Free} - Fs \text{ in the supernatants}}{Fs \text{ initial content}} \times 100 \quad (2)$$

Where, CN and Fs are the initial contents which are added to fabricate the gels, where the free-CN, free-Fs are the remaining in the supernatants.

2.7. Structural characterization

2.7.1. UV-vis spectroscopy

The UV absorption of Cs-gel, Fs (3 mg/mL), CN, CCN, and CCF-9 were examined using UV/vis spectroscopy (UV-8000, Metash Instruments, Shanghai, China). 2 mg/mL of gel was aliquoted and dissolved in PBS (pH 7.4), then centrifuged at 1677×g for 7 min. Supernatants of all samples were collected and measured at a wavelength ranging from 200 to 400 nm.

2.7.2. FTIR

The functional groups of CN and Fs loaded on CN-nanoparticles were investigated. The lyophilized gel (5 mg) was analyzed using FT-IR IS50 (Thermo Fisher Scientific, US) in the wavenumber range of 1000–4000 cm^{-1} . The scanning was performed at a minimum rate of 21 min^{-1} with a resolution of 2 cm^{-1} . The baseline of the FTIR spectra was established using the Omnic program. To determine the quantity of the component bands, we performed second derivative calculations and a multiple Gaussian curve-fitting analysis using Peak Fit software version 4.12 (SPSS Inc., Chicago, IL, US).

2.7.3. Raman spectroscopy

The gels were analyzed using Horiba Optics Inc.'s Raman spectroscopy apparatus (France), which had a 100-mW laser with a wavelength of 633 nm. The range of 500–4000 cm^{-1} , 32 scans, and 4 cm^{-1} spectral resolution were used for the data collecting process.

2.7.4. XRD analysis

The crystalline and amorphous content of prepared Cs, CCN, and CCF-5 was analyzed using Malvern Panalytical's multifunctional powder diffractometer (XPert Pro MPD). 20 mg of each sample was scanned at a rate of 4° min^{-1} in the region from 5 to 80° at 40 kV and the tube current was adjusted at 40 mA. The crystalline size of samples was determined by the Scherrer's equation as follow:

$$D = \frac{K\lambda}{\beta \cos \theta} \quad (3)$$

Where, D represents the crystalline size of the samples, K is the Scherrer constant, λ is the wavelength of X-ray source, β is the radians, and θ is the peak position.

2.7.5. XPS analysis

The samples were measured using an electron spectrometer, and the XPS spectra were calibrated using a reference energy value of 284.8 eV (Ciobanu et al., 2023). The XPS data were analyzed using the Thermo-Avantage program. Gaussian curve-fitting analysis was used to fit all peaks by Origin version 2024b (Origin Lab, Co., US), with a Jiangsu University accessibility.

2.7.6. SEM

The morphology of Cs, CCN, and CCF-9 was analyzed using SEM (JSM-7001F, JEOL Co., Japan). The freeze-dried samples were placed onto an aluminum plate, and an accelerating voltage of 5 kV was applied. Three different magnifications of 30, 50, and 70 kx were used to examine the gel morphology. The elemental composition of the samples was evaluated throughout the SEM process using an energy dispersive X-ray spectrometer (EDX). Moreover, the particles size distribution gained from SEM snapshots was extracted by ImageJ and then their histogram was plotted and fitted by OriginLab 2024b.

2.8. Determination of the in vitro antioxidant activity

2.8.1. DPPH-scavenging activity

The DPPH scavenging activity was used to test the capabilities of Cs, CCN, CCF-3, CCF-5, CCF-7, and CCF-9. CN (250 $\mu\text{g/mL}$) and various concentrations of Fs (3, 5, 7, and 9 mg/mL), referred to Fs-3, Fs-5, Fs-7, and Fs-9, respectively (Salah et al., 2020). Initially, 0.4 mL of the prepared gel was dissolved in acetic acid (1%) and combined with 1.8 mL of DPPH (0.2 mM) in an EtOH solution. The reaction solution was incubated for 0.5 h with agitation at room temperature in a dark environment. The samples were subjected to centrifugation at a speed of 2415×g for 10 min. Subsequently, the UV-absorption reaction solution was quantified at a wavelength of 517 nm using a microplate reader (Multiskan Go, Thermo Scientific, China). Ascorbic acid served as the standard equivalent, and was measured in ASE ($\mu\text{g/mL}$). Thus, the DPPH radical-scavenging activity of samples was calculated using the following equation:

$$DPPH \text{ Scavenging activity } (\%) = \frac{C - \text{Abs}}{C} \times 100 \quad (4)$$

Where, Abs represents the absorbance of the samples, and C is the absorbance of control.

2.8.2. ABTS-radical scavenging activity

A solution of ABTS free radical (7 mM) was combined with potassium persulfate (2.45 mM) and prepared in PBS (10 mM, pH 7.4) at room temperature (Li et al., 2018). The UV-absorption of solution was diluted until ABS absorption reached 0.7. 0.4 mL of the prepared gel was suspended in acetic acid (1%) before mixing with 1.8 mL of the ABTS free radical solution. It was then incubated, centrifuged at 2415 ×g for 10 min, and scanned at 734 nm. The standard curve equivalent of ascorbic acid ASE ($\mu\text{g/mL}$) was used. The ABTS + scavenging activity (%) was calculated using the following equation:

$$ABTS \text{ Scavenging activity } (\%) = \frac{C - \text{Abs}}{C} \times 100 \quad (5)$$

Where, Abs denotes the absorbance of the ABTS free radical solution, and C is the absorbance of control.

2.9. Antimicrobial of CN and Fs loaded on Cs-gel

2.9.1. In vitro antifungal assay

P. expansum 3.3703, obtained from moldy apples, was acquired from the China General Microbiological Culture Collection Centre. *A. westerdijkiae* fc-1 strain was provided by the Chinese Academy of Agricultural Sciences. Fungi were cultivated in potato dextrose agar (PDA) using sterile dH_2O in a sterile environment for a well-diffusion

method (Do et al., 2022). Fungal spores were diluted at 1×10^6 and mixed with sterile H₂O (as a control), Cs, CCN, CCF-3, CCF-5, CCF-7, and CCF-9 gels. All treatments were incubated for 4 h in the dark, and 30 μ L were injected into the sterile PDA. Inoculated plates were then incubated at 25 °C for 7 days, and the zone of inhibition (%) was determined.

$$\text{Inhibition (\%)} = \frac{\text{Control diameter} - \text{Treatment diameter}}{\text{Control diameter}} \times 100 \quad (6)$$

2.9.2. In-vitro antibacterial assay

B. cereus (ATCC 10987), *E. coli* (ATCC 8739), and *S. aureus* (ATCC 6538A) were bought from the National Research Centre (NRC) located in Cairo, Egypt. All bacterial strains were pre-cultured in nutrient broth medium for 12 h and total counts of bacterial strains were adjusted at $1 \times (10^6-10^7)$ using a dilution assay (Wu et al., 2023). Briefly, 100 μ L of each bacterial broth was equally spread on a nutrient agar plate. Then, filter papers were soaked with Cs, CCN, CCF-3, CCF-5, CCF-7, and CCF-9 gels for 5 min. These filter papers (6 mm) were put on the bacteria plates which were then incubated for 24 h at a temperature of 37 °C. The antibacterial activity was presented in the form of the zone-inhibition (mm), and antibacterial activity rate (%) which was calculated as per the following equation:

$$\text{Antibacterial rate (\%)} = \frac{C - T}{C} \times 100 \quad (7)$$

Where, C is the colony count of bacteria strain before mixing with samples and T is the colony count of bacteria strain after treating with samples.

2.10. Texture analysis of prepared gels

Texture profile analysis (TPA) of Cs, CCN, CCF-9 gels were assessed via a TA-TX plus (texture analyzer Stable, Micro Systems Ltd., Surrey, UK), attached with a load cell (5-kg). All samples were tested using a trigger force of 5 g, a pre-test speed of 1 mm/s, a test speed of 1 mm/s, and a post-test speed of 1 mm/s (Athipornchai et al., 2024). The hardness (g), adhesiveness (g. sec), cohesion (%), resilience (%), springiness (%), chewiness, and gumminess were calculated at 25 °C.

2.11. Release profile assay

The release behavior of Fs from CCF-3, CCF-5, CCF-7, and CCF-9 were measured. The prepared gel was dissolved in 10 mL PBS solution (pH 7.4), and each treatment was incubated at 37 °C with shaking. Then, 2 mL of each treatment was measured by UV-vis spectroscopy at 280 nm (Phonrachom et al., 2023). Simultaneously, 2 mL of PBS was added to each treatment equal its original volume.

2.12. Molecular docking modeling

The binding among the gel matrices was theoretically evaluated using molecular docking approach. The initial geometry of chitosan (PubChem CID: 71853), cinnamaldehyde (PubChem CID: 637511), narirutin (PubChem CID: 442431), phytic acid (PubChem CID: 890), and pentsodium triphosphate (PubChem CID: 24455) was acquired from PubChem database (<https://pubchem.ncbi.nlm.nih.gov/>) and optimized by SYBYL X-2.0 on a windows operating system. The energy minimization of each structure was conducted by the Powell method using Tripos force field, where a convergence criterion of 0.005 kcal/(mol Å) was used as the termination of the Powell conjugate gradient algorithm. The maximum iterations were set to 1000 steps and the other parameters were defaulting adjusted (Khalifa et al., 2021). Molecular docking study was done by Surflex-dock model using the lowest-energy conformations. H₂O and bound ligands were removed from the receptor prior to docking analysis and all parameters were default. After successful docking, all the putative docking models were analyzed and

selected based on H-bonding. The stabilized structure served to visualize the capability to form H-bonding, and to determine the sites and number of direct and intermediate H-bonding. Oppositely, geometry of the initial molecules and complexes were further optimized using M062X function with 6-31G (d, p) basis set, which was implemented in Gaussian 09 package to calculate theoretical thermodynamic constants. The binding constants and driving forces were finally computed.

2.13. Statistical analysis

All tests were done in triplicate, and the outputs were stated as the mean value \pm SD. Statistical analysis was done using SPSS 27.0 (SPSS Inc., CHI, US), including one-way analysis of variance (ANOVA) with Duncan's post-hoc test to compare the mean values at a significance level of $p < 0.05$. The educational version of OriginPro (2024b) was used to draw and present the data. The software Minitab, version 16 (Minitab, Inc., US) was used to perform the principal component analysis (PCA). Using Origin 2024b (Origin Lab, Co., US), with a Jiangsu University accessibility, a bubbles Pearson correlation study was conducted with significance levels of 0.05, 0.01, and 0.001.

3. Results and discussion

3.1. The interaction of CN and Fs loaded on Cs

The yield of flavonoid extract after lyophilization was $8.95 \pm 0.039\%$, and TFC was 6.10 ± 0.245 mg rutin/g dry flavonoid extract. The results revealed for the high EE at high level of Fs loaded on CCN, as presented in Table S1. The EE of CCF ranged from 75.95 ± 1.74 to $83.14 \pm 3.34\%$, with an increase in flavonoid level, while EE of CCN was $80.56 \pm 1.17\%$. The maximum EE for CCF-9 was $83.14 \pm 3.34\%$. This manifests that Cs-gel successfully encapsulates Fs, with a dose-dependent EE, showing the suitability of Cs-gel to encapsulate CN and Fs. The high encapsulation of CCF-9 is due to the existence of many OH-groups in flavonoid molecules, which could interact with the positive charge on the surface of chitosan through electrostatic interaction (Aluani et al., 2017). Roy et al. (2019) exhibited that the EE of quercetin and myricetin encapsulated in the chitosan matrix was 81 and 89%, respectively agreeing with our results. Furthermore, these differences in EE may be ascribed to the pH levels, the ratio of chitosan to cross-linker agent, the concentration of phytochemicals, and the polymer's binding affinity toward active components, as previously reported by Sun et al. (2020). The interaction between Cs-gel and CN and Fs was then examined using UV-vis, FTIR, and XRD assays.

The structure of flavonoids consists of two separate bands. Band I correspond to the cinnamoyl group, which includes the B ring and part of the C ring which was observed at wavelengths between 300 and 380 nm. Band II corresponds to the benzoyl group, which includes the A ring and part of the C ring which was observed at wavelengths between 240 and 280 nm (Duan, 2014). The UV spectrum of Fs (5 mg/mL) shows two bands at 310–360 nm and the other at 260–280 nm (Fig. 1A). However, these bands disappeared in the UV spectrum of CCF-5, confirming that Fs might be entrapped into chitosan matrix. Additionally, the UV-spectra intensity of CCF-5 was increased, compared with the Cs-gel spectrum likely attributed to the binding of the cinnamoyl part of Fs with Cs-gel. Zhang et al. (2008) reported that the band II disappeared after loading quercetin on chitosan-nanoparticles. Fig. 1B shows that the spectrum of CN displayed a band around 270–295, which is related to the benzene molecule conjugated with a C=O group (Cox et al., 2021). Similar results were observed in the UV spectrum of CCN gel. The peak position changes are due to the interaction between the CN band and Cs-gel, as previously reported (Wu et al., 2023). These results confirmed the binding and integration of Fs or CN into Cs matrix during gelation.

FTIR spectroscopy was employed to assess functional groups involved in the interaction between the carriers and bioactive substances. FTIR of Fs (5 mg/mL), CN (250 μ g/mL), prepared gel of CCF-5,

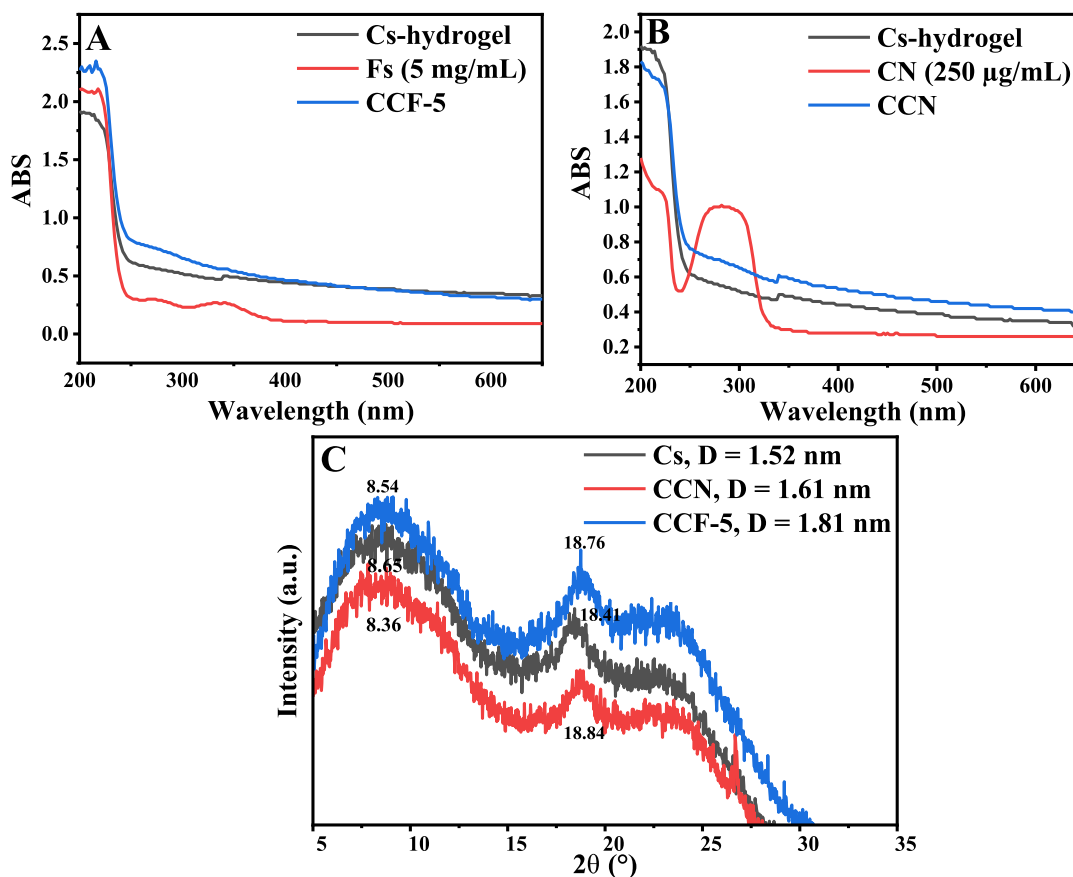


Fig. 1. A) Uv-absorption of Cs-hydrogel, Fs (5 mg/mL), and CCF-5, B) Uv-absorption of CN (250 µg/mL) and C) XRD patterns and crystalline size (D, nm) of Cs-hydrogel, CCN, and CCF-5. Where CCF-5 means that Fs (5 mg/mL) loaded on CCN, While CCN is CN (250 µg/mL) loaded on Cs-gel.

CCN, and Cs are shown in Fig. 2A. The Cs-gel exhibited two distinct absorption peaks at 3292.53 and 1635.98 cm^{-1} , corresponding to the stretching vibration of -O-H, broad signal and the amide-I groups (=N-H, acute signal), respectively. Nalini et al. (2022) showed that the peak absorption at 3200–3500 and 1635–1690 cm^{-1} referred to H-bonds and amide-I, respectively. FTIR signal of Fs shows a peak at 3320.26 cm^{-1} , demonstrating to the O-H-group, while the sharp signal of the peak at 2972.26 cm^{-1} corresponded to the C-H vibration. The FTIR spectrum of CN showed two distinct sharp bands at 1668.82 and 1624.82 cm^{-1} , corresponding to C=O which is related to the CHO-group and aromatic benzene ring linked with C=H. The binding of CN and Fs on Cs-gel induced H-bond formation, resulting in peak shift as reported by Liu et al. (2020). The O-H-group band was red-shifted to 3301.54 and 3304.02 cm^{-1} in the CCN and CCF-5 spectra, respectively, signifying the formation of new hydrogen bonds within the initial binary complex through the process of ionic-gelation. (Liang et al., 2021). The disappearance of bands at 1668.82, 1624.82, and 2972.65 cm^{-1} in the CCN and CCF-5 spectra further inferred the presence of hydrogen bonding formation between Fs or CN with Cs-gel. Furthermore, the peak intensity changes confirmed the interaction of CN and Fs with the Cs-gel. The findings exhibited that encapsulating bioactive materials in glycopolymer based on nanoparticles led to the formation of H-bonds as manifested by significant shift in the peak intensity. As observed in Fig. 2B, the peak fit analysis of amid-1 (1620–1650 cm^{-1}) showed 5, 4, and 3 stretching small peaks of Cs, CCN, and CCF-5 gels, respectively. Briefly, all the analyzed fitted peaks were derived from the amid-1 peak, but the secondary structure, including α -helix, β -turn, and so on, led to the amid-1 peak producing some fine peaks. These findings revealed that Fs and CN could greatly influence the secondary structure of Cs-gel, mostly due to their interaction together. To gain a greater understanding of the bonding arrangement of CN and Fs integrated with Cs-gel, Raman

spectroscopy was conducted. Fig. 2C displays the Raman spectra of Cs, CCN, CCF-3, CCF-5, CCF-7, and CCF-9 gels. It was observed that C-C (1000–1250 cm^{-1}) stretching region in Cs-gel structure was influenced by the integration of CN and Fs. In comparing with Cs-gel, the CC stretching peak intensity of CCF-3 to CCF-9 was increased. This indicated that the Fs successfully interacted with CCN-gel (Fig. 2C). Similar phenomena were observed when CN encapsulated into Cs-gel (Fig. 2D). Jha and Mayanovic (2023) have shown that conformational changes can cause modest effects in the Raman spectra, such as frequency shifts, changes in intensity, and broadening of the relevant Raman bands. These data were in agreement with the above results of Uv-vis and FTIR.

3.2. XRD, XPS analysis and the morphology of Cs, CCN, and CCF-5

The X-ray diffraction (XRD) patterns were performed for CN, CCN, and CCF-5, as displayed in Fig. 1C. In general, diffraction patterns showed that the crystalline materials present in the sample exhibit sharp peaks, while broad peaks indicated the presence of amorphous materials (Liang et al., 2021). The diffractogram of Cs, CCN, and CCF-5 revealed two distinct peaks at 8.65° and 18.41°, 8.36° and 18.84°, and 8.54° and 18.76°, respectively. These peaks showed that all prepared samples were in an amorphous state. Moreover, the crystalline size of Cs, CCN, CCF-5 were 1.52, 1.61, and 1.81 nm, respectively. Comparing Cs with the CCF-5 and CCN diffractograms, the peaks were slightly red-shifted. Moreover, changes in peak intensity suggested that the hydrogen bonding between CN and Fs with Cs occurred. These findings indicated that the distances between the chains expanded and the H-bond of the amorphous Cs was disrupted in an irregular manner as previously reported (Chen et al., 2016). Liu et al. (2020) observed that the diffractogram peaks became broader after encapsulating CN into whey protein isolate-dextran complex and chondroitin sulfate. Similar

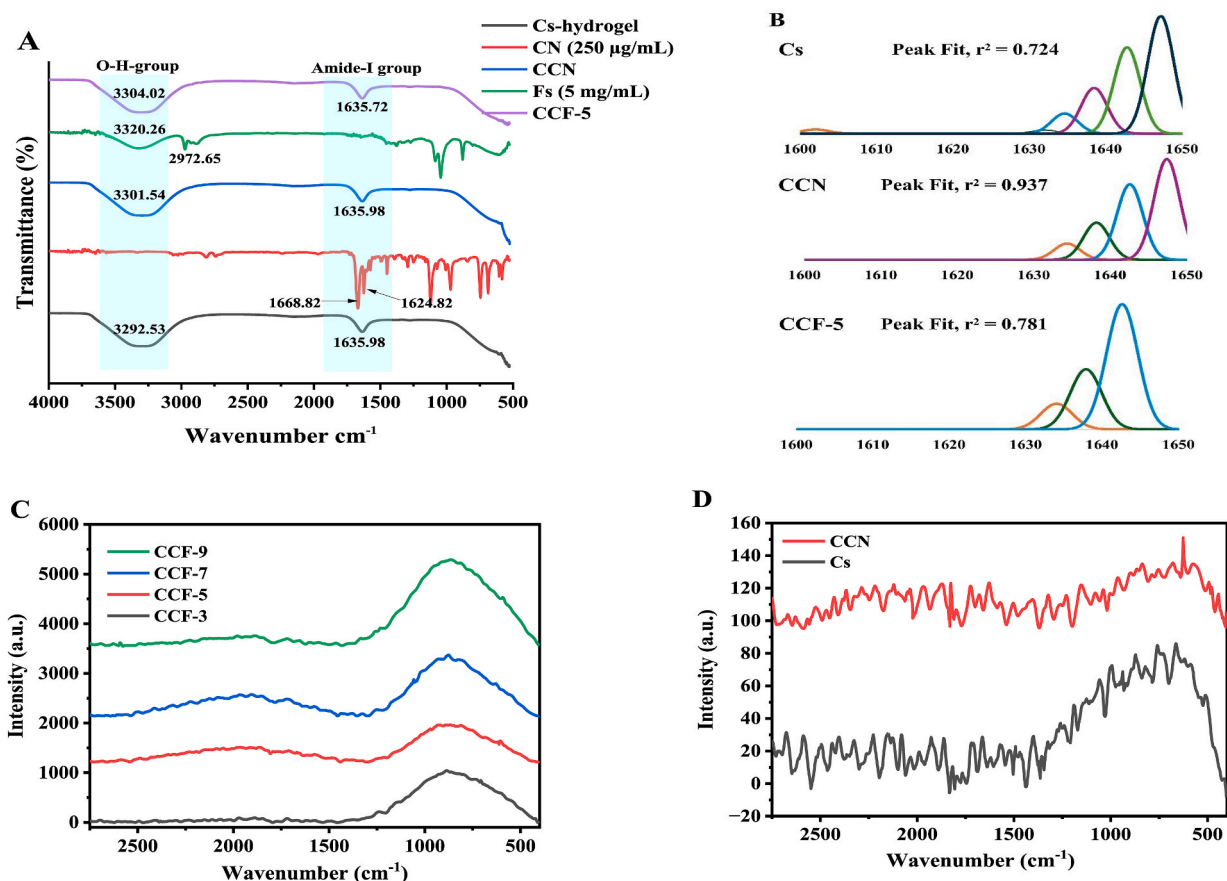


Fig. 2. A) FTIR of Fs (5 mg/mL), CN (250 µg/mL), CCF-5, CCN and Cs, B) peak fit of amide-I (1620-1650 cm^{-1}) of Cs, CCN, and CCF-5 gels, C) Raman spectroscopy of CCF-3, CCF-5, CCF-7, and CCF-9 gel, and D). Cs, CCN-gel.

phenomena were reported by Ding et al. (2021), who implied that the amorphous state contributed to the H-bond formation of the chitosan-proanthocyanidin interaction. These results showed that the H-bond controlled the interaction of CN and Fs with Cs-matrix which was in accordance with FTIR results. Fig. 3 shows the XPS spectra of Cs, CCN, and CCF-5 gel, where the binding energy ranges from 0 to 1200 eV. The elements scanned in the Cs, CCN, and CCF-5 gel structures were carbon (C), oxygen (O), and nitrogen (N) (Jiang et al., 2024). Meanwhile, sodium (Na) and phosphorus (P) involved in the gel formation contributed to the cross-linkers (tripolyphosphate and phytic acid) that are used to bind CN and Fs. After cross-linking by tripolyphosphate, the CCN gel contains Na and P, as observed in the XPS spectra (Fig. 3A and C). After cross-linking with phytic acid, the CCF-5 gel contains only P, as shown in the XPS spectra in Fig. 3A and D. Moreover, Fig. 3B, C, and D display the element resolution of C1s, O1s, N1s, Na1s, and P2p in Cs, CCN, and CCF-5 gels. All gels in the C1s spectra display different binding energies at 284.4, 286, and 282.8 eV, contributing to the C-C/C-H/C=C, C-OH/C-O-C, and C-C/C=C groups. While N1s spectra show levels at 399.4 and 397.3, mostly contributing to C-N/NH-C-O and C-N groups, notably, CCN and CCF-5 had a different N (count/s) content than Cs-gel, indicating the formation of Schiff base. Similarly, the different content in the O1s spectrum could correspond to the formation of the CHO group in CCN and CCF-5 gels. Similar phenomena were reported by Zhou et al. (2024). This result indicated that CN and Fs were successfully encapsulated into the Cs-gel structure.

SEM was used to investigate the morphology of the dried Cs, CCN, and CCF-9, as shown in Fig. 4. The Cs morphology was squishy and porous, which confirms the presence of gelation using a cross-linking agent. At 70 KV magnification, the micrographs of CCN showed a little crust with less porous surfaces covered with flake grains due to ionic

crosslinking agent (TPP) binding with CN and Cs. At 70 KV magnification, the CCF-9 micrographs showed a crusty shape and an almost non-porous surface, indicating that Fs was successfully embedded inside the CCN matrix. Moreover, the particle sizes found in the Cs-gel were in the range of 0.2–0.75 µm. A larger number of particles are found between 0.35 and 0.55 µm, while a smaller number of particles are found between 0.550 and 0.75 µm. Similar observations were made for the particle size distribution of CCN and CCF-5 observed from SEM images, as shown in Fig. 5. These structures can enhance the interface contact with the core material and generate a multi-dispersed microstructure (Li et al., 2024). Furthermore, atoms (%) obtained from EDX revealed that Cs, CCN, and CCF-5 have high contents of carbon and oxygen ions. Post loading of CN and Fs on the Cs matrix, the atom percentage of carbon ions increased in the order of Cs < CCN < CCF-5. This demonstrated that CN and Fs bonded the C-H chain of Cs with a new carbon chain as reported by Athipornchai et al. (2024).

3.3. Antioxidant activity in-vitro

The scavenging activities of all gels against DPPH and ABTS free radicals were also confirmed using ascorbic acid equivalent (ASE, µg/mL) as displayed in Fig. 6. The data demonstrated that DPPH-scavenging activity of Fs ranged from 42.12 ± 0.48 to 61.02 ± 1.80 µg/mL using 3 and 9 mg/mL, respectively (Fig. 6A). After loading CN, the antioxidant ability of CCN was 3.06 ± 1.51 µg/mL, which was higher than Cs-alone, suggesting that CN may improve Cs' scavenging ability against DPPH free radicals. Likewise, upon loading flavonoids on CCN structure, the abilities of CCF-3, CCF-5, CCF-7, and CCF-9 were 15.30 ± 0.66 , 24.58 ± 0.53 , 32.84 ± 0.42 , and 38.22 ± 0.37 µg/mL, respectively. The highest antioxidant capacity against DPPH free radical was observed at $38.22 \pm$

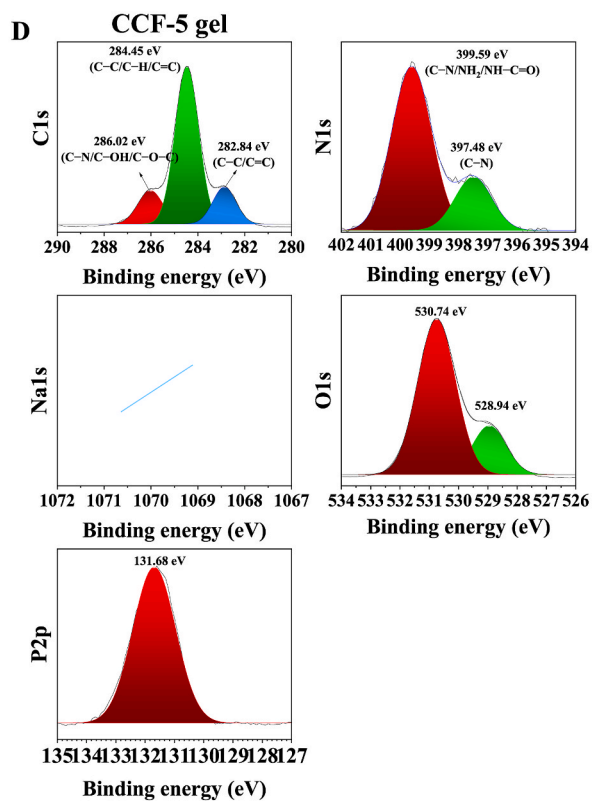
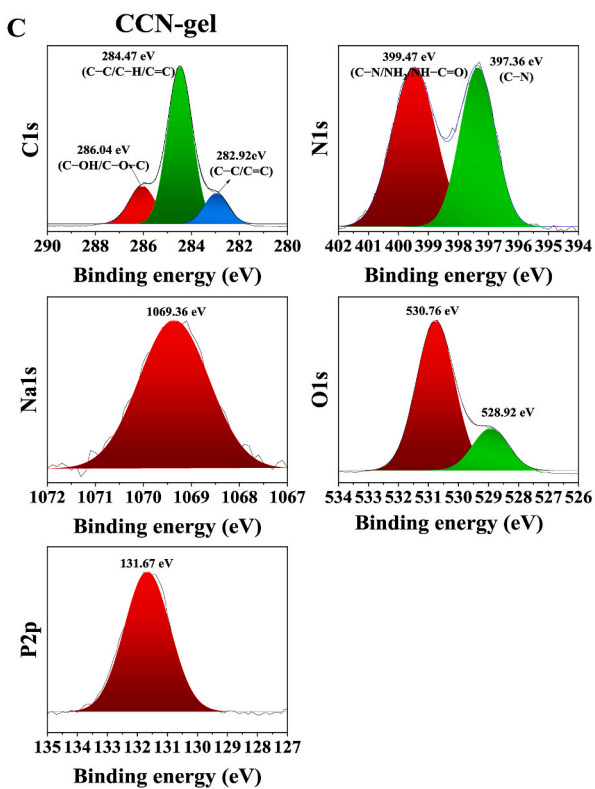
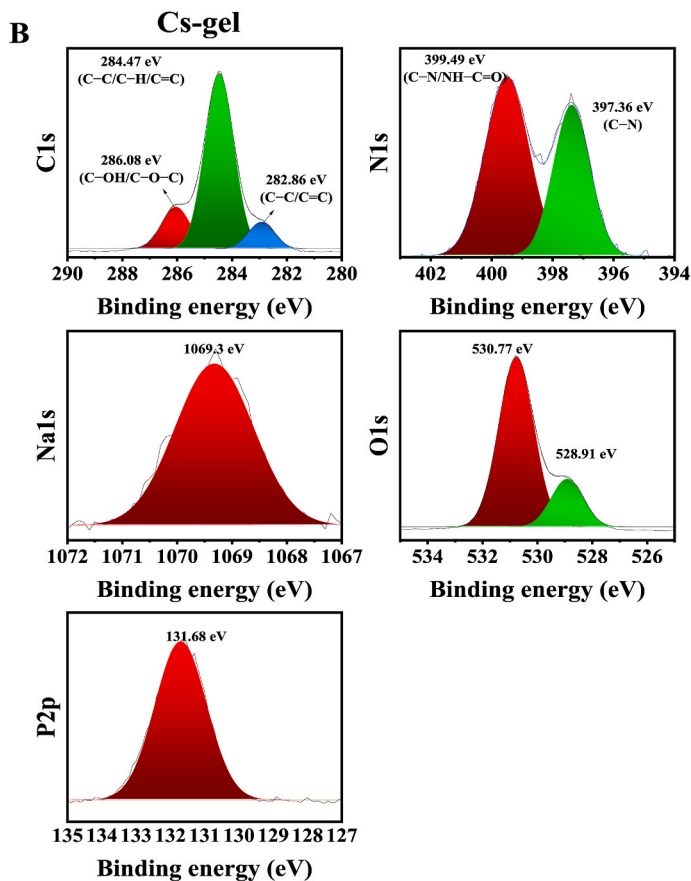
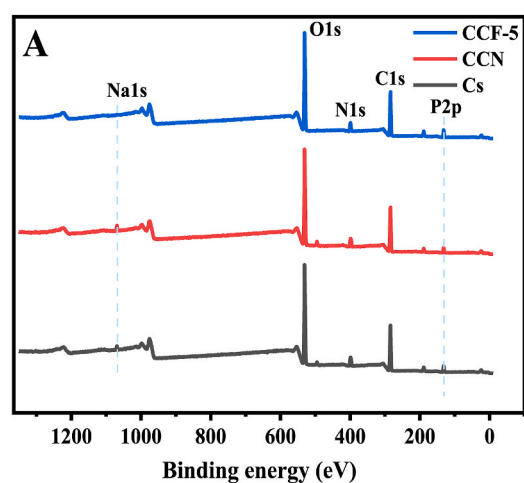


Fig. 3. XPS wide-scan spectra obtained for Cs, CCN and CCF-5 gel (A), XPS high-resolution spectra of C1s, O1s, N1s, Na1s and P2p obtained for Cs (B), CCN (C) and CCF-5 (D) gel.

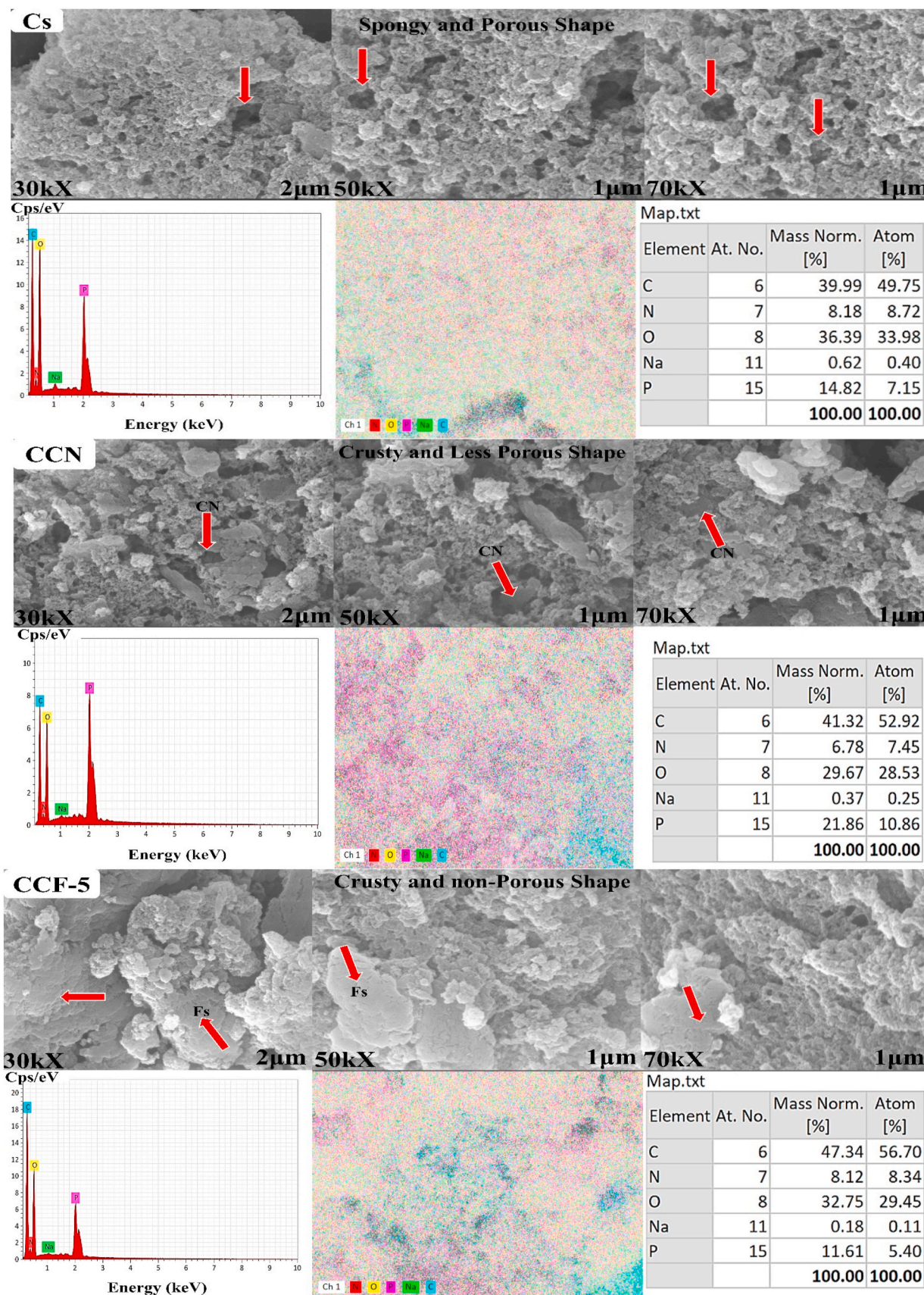


Fig. 4. SEM micrographs and elemental composition by EDX of Cs, CCN, and CCF-5. Where CCF-5 means that the Fs (5 mg/mL) loaded on CCN, While CCN is CN (250 µg/mL) loaded on Cs-gel.

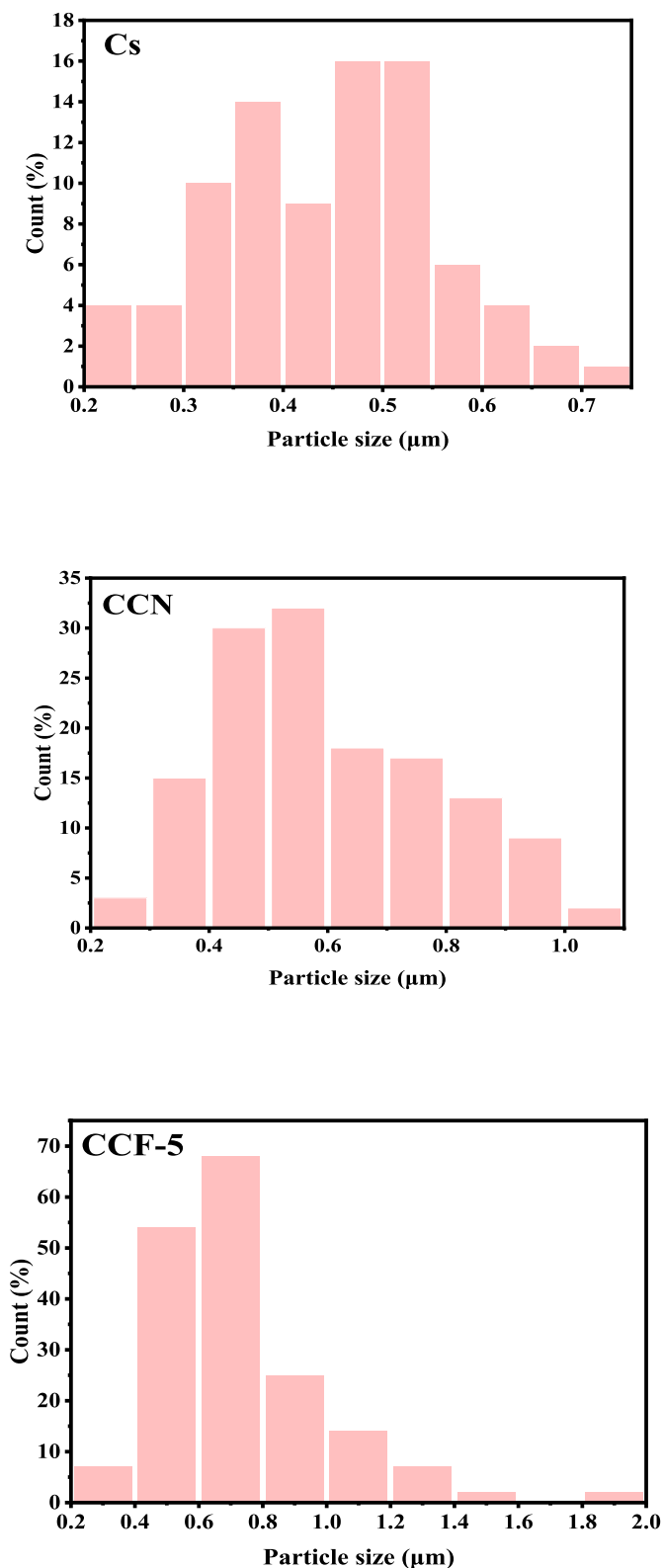


Fig. 5. Particle size distribution histogram plot for Cs, CCN, and CCF-5 gels.

0.37 μg/mL for CCF-9 gel. Salah et al. (2020) showed that the antioxidant activity of purified anthocyanin’s extract is dose dependent. This outcome might also be associated with the fact that the binding of Fs or CN in the Cs-gel permitted Fs or CN to be more readily immersed in the DPPH solution, thus increasing the reaction contact with the free radical (Liang et al., 2021). Furthermore, the variation in the scavenging

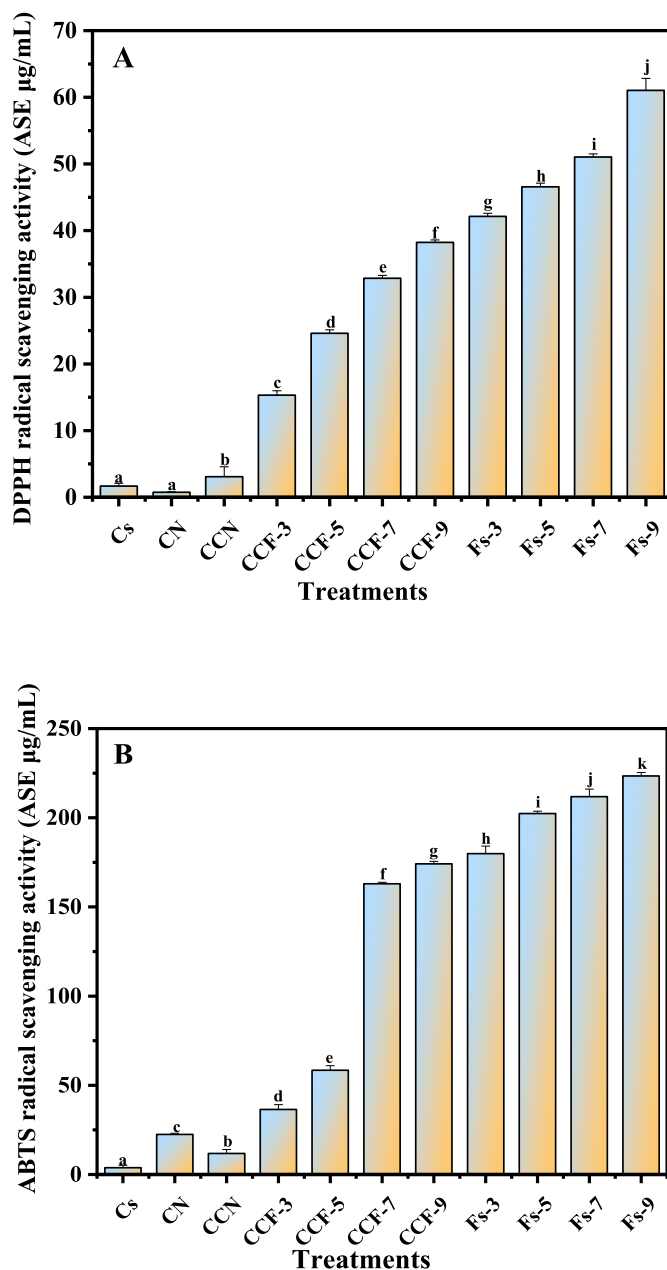


Fig. 6. *In vitro* antioxidant activity using (A) DPPH radical scavenging and (B) ABTS radical scavenging assays. The Fs loaded on CCN gel was designated as (3 mg/mL, CCF-3), (5 mg/mL, CCF-5), (7 mg/mL, CCF-7) and (9 mg/mL, CCF-9). Where Fs-3, Fs-5, Fs-7, and Fs-9 were the free of unloaded Fs. While CCN is CN (250 μg/mL) loaded on Cs-gel. Values represent mean and ± standard deviation of three replicates. Different letters on the bars indicate significant differences among the samples ($p < 0.05$).

activity was more consistent with EE % findings, suggesting that Fs and CN interacted with the Cs matrix. The ABTS scavenging activity of CCF-3, CCF-3, CCF-5, CCF-7, and CCF-9 were 36.43 ± 2.73 , 58.42 ± 2.58 , 163 ± 0.81 , and 174.170 ± 1.36 μg/mL, respectively (Fig. 6B). The highest scavenging ability against ABTS free radical was 174.170 ± 1.36 μg/mL for CCF-9 gel. Ding et al. (2021) found that the antioxidant ability of Cs-nanoparticles fabricated by gelation method with the aid of TPP was limited. Besides the high molecular weight of chitosan, it is evident that the TPP cross-linker quenched the amino acid group inside the chitosan structure and prevented this functional group from reacting with ABTS or DPPH free radicals. The produced gel exhibited a stronger ABTS scavenging activity compared to the DPPH scavenging activity

attributed to the fact that ABTS radicals can dissolve in both water and organic solvents, allowing for the assessment of the antioxidant capacity of both hydrophilic and lipophilic molecules. Chen et al. (2023) showed that the ability of anthocyanins loaded on chitosan/ β -lactoglobulin to scavenge the ABTS free radicals was higher than DPPH free radical. Furthermore, the variation in the scavenging activity is more consistent with the EE% findings, suggesting that Fs and CN interact with the Cs matrix and have the potential to exert their antimicrobial activity.

3.4. Antimicrobial activity in vitro

The cultivation of fungus on solid media has numerous advantages, including the ease and cost-effectiveness of the assay, as well as the ability to evaluate a wide range of antimicrobial compounds. Fig. 7A shows the antifungal activity of Cs, CCN, CCF-3, CCF-5, CCF-7, and CCF-9 gels against *P. expansum* and *A. westerdijkiae*. After loading Fs on CCN gel, the inhibition (%) of CCF-3, CCF-5, CCF-7, CCF-9 against *A. westerdijkiae* were 48.22 ± 2.45 , 56.73 ± 1.22 , 75.17 ± 12.28 , and $93.61 \pm 2.12\%$, respectively, Fig. 7B. However, the inhibition (%) against *P. expansum* was limited and still significant between the treatments of CCN, CCF-3, CCF-5, CCF-7, and Cs-gel. Additionally, CCF-9 gel showed a significant inhibition on the spore growth of *P. expansum*, while the growth of mostly *A. westerdijkiae* was inhibited. The corresponding inhibition (%) of CCF-9 against *P. expansum* and *A. westerdijkiae* were 29.91 ± 1.22 and $93.61 \pm 2.12\%$, respectively indicating that CCF-9 exhibited a stronger effect against *A. westerdijkiae* than *P. expansum*, compared with Cs-gel. These results demonstrated

that the biologically active components enhanced Cs structure and effectively inhibited the extension of the fungus colony diameter. Flavonoids exhibit antifungal properties via inducing alterations in the structure of fungal cell walls and endomembrane system, thereby, inhibiting fungal growth and activity (Liu et al., 2021). The antibacterial ability of Cs, CCN, CCF-3, CCF-5, CCF-7, and CCF-9 gels against *S. aureus*, *E. coli*, and *B. cereus* is shown in Fig. 8A. The antibacterial diameter zones of Cs, CCN, CCF-3, CCF-5, CCF-7, and CCF-9 against *E. coli* were 16.25 ± 0.06 , 17.65 ± 0.04 , 19.7 ± 0.05 , 21.15 ± 0.04 , 22.70 ± 0.05 , and 26.16 ± 0.02 mm, respectively (Fig. 8B). While the inhibition zones of Cs, CCN, CCF-3, CCF-5, CCF-7, and CCF-9 against *B. cereus* were 12.33 ± 0.57 , 15.81 ± 0.23 , 14.33 ± 0.15 , 15.47 ± 0.02 , 19.60 ± 0.05 , and 27.69 ± 0.05 mm, respectively. Li et al. (2018) exhibited that the inhibition diameter of Cs against *S. aureus* and *E. coli* ranged from 7 to 11 mm, and in agreement with our results. Furthermore, the prepared CCF-9 gel, at the highest concentration of Fs, showed antibacterial abilities against the three pathogenic bacteria in the following order: *S. aureus* > *B. cereus* > *E. coli*. The corresponding diameters of the antibacterial zone were at 28.65 ± 0.05 , 27.69 ± 0.04 , and 26.16 ± 0.02 mm, respectively inferring that Fs embedded in CCN exerted a significant effect on the antibacterial effect. A previous study showed that the licoricidin (iso-flavonoid) loaded on chitosan has a good antimicrobial ability against pathogenic microbes (Wu et al., 2023). Moreover, the results confirm that the activity of Cs-gel was enhanced by binding to CN and Fs. The action mechanism might be attributed to the fact that the fabricated CN and Fs with Cs-gel have unique structures that prevent nutrients uptake and inhibit pathogenic bacteria as

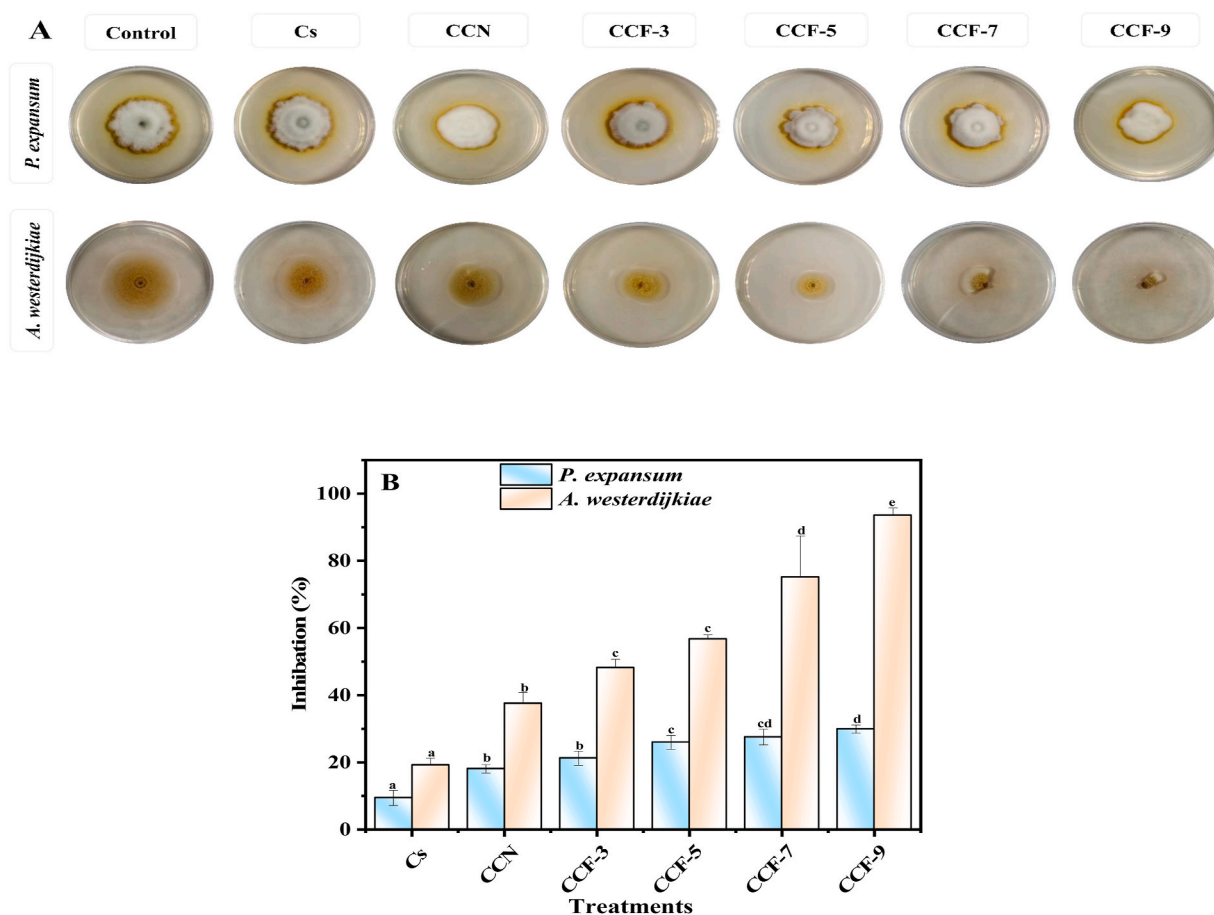


Fig. 7. *In vitro* antifungal activity as presented by (A) fungi colony after 7 d and (B) inhibition (%) of Cs, (CN 250 μ g/mL loaded on Cs-gel, CCN), (Fs 3 mg/mL loaded on CCN, CCF-3), (Fs 5 mg/mL loaded on CCN, CCF-5), (Fs 7 mg/mL loaded on CCN, CCF-7) and (Fs 9 mg/mL loaded on CCN, CCF-9) against *P. expansum*, *A. westerdijkiae*. Values represent mean and \pm standard deviation of three replicates. Different letters on the same type of bar indicate significant differences among the samples ($p < 0.05$).

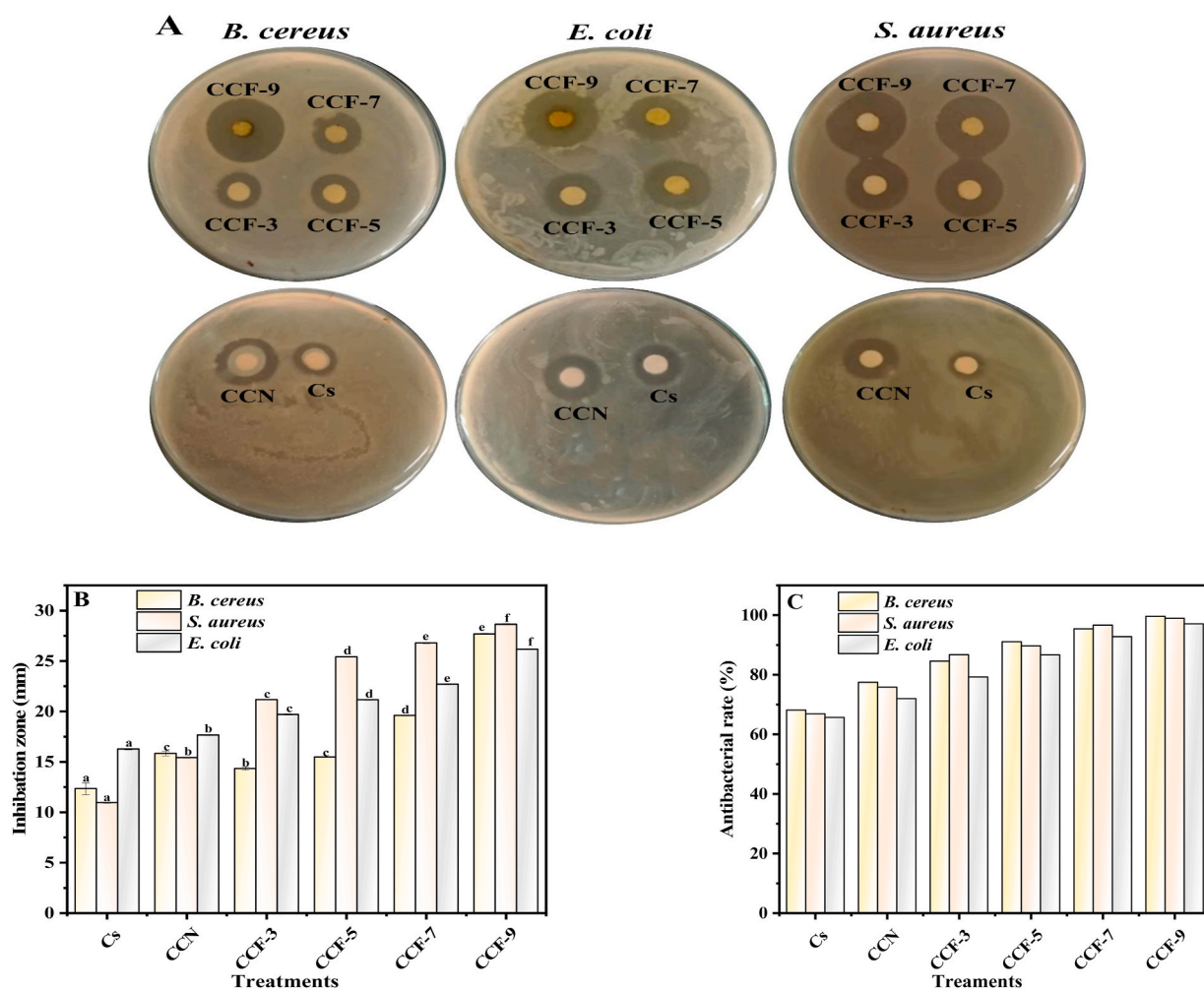


Fig. 8. *In vitro* antibacterial activity as presented by (A) bacteria colony growth after 24 h and (B) inhibition zone and (C) Inhibition rate (%) of Cs, (CN 250 $\mu\text{g}/\text{mL}$ loaded on Cs-gel, CCN), (Fs 3 mg/mL loaded on CCN, CCF-3), (Fs 5 mg/mL loaded on CCN, CCF-5), (Fs 7 mg/mL loaded on CCN, CCF-7) and (Fs 9 mg/mL loaded on CCN, CCF-9) against *B. cereus*, *S. aureus*, and *E. coli*. Values represent mean and \pm standard deviation of three replicates. Different letters in the same type of bar indicates significant differences among the samples ($p < 0.05$).

previously reported (Zhou et al., 2024). The antibacterial effect (%) of prepared gels against these bacteria strains was also investigated. As shown in Fig. 8C, the prepared gels exhibited antibacterial rate (%) in the following order: CCF-9 > CCF-7 > CCF-5 > CCF-3 > CCN > Cs, which are in line with the inhibition diameter zone. Previous studies indicated that the antibacterial rate (%) of free-Cs against *S. aureus* and *E. coli* was 60 and 40%, respectively (Wang et al., 2023). Overall, *in-vitro* antimicrobial assay results indicated that the binding of CN and Fs on Cs-gel has potential for use as an antimicrobial agent.

3.5. Texture profile analysis (TPA)







The TPA factors of Cs, CCN, CCF-3, CCF-5, CCF-7, and CCF-9 gels as key, control, and reference samples are displayed in Table 1. Hardness is the most important physical characteristic of fabricated gel. Among all prepared gels, hardness ranged from 55.29 ± 2.23 to 152.66 ± 3.18 g. After loading the Fs on CCN-gel, the hardness increased in the order CCF-3 < CCF-5 < CCF-7 < CCF-9. However, after loading CN onto Cs-gel, the hardness of CCN decreased, likely attributed due to hydrogen bond formation upon Fs embedding inside the CCN gel. Zhong et al. (2022) reported that the binding of different flavonoid molecules exhibited an effect on the hardness of ovalbumin hydrogel. Furthermore, the presence of an ordered Cs-gel structure increased the hardness level (Khorshidi et al., 2023). Springiness (%) is well-defined as the elasticity

of prepared gels which showed an increase upon the addition of CN and Fs to Cs-gel. The springiness (%) of prepared gels ranged from 19.43 ± 0.50 to 47.69 ± 2.19 %. It was observed that the chitosan structure may improve the elasticity levels, which would help to use this gel in food candy industry. The variation in elasticity of CN and Fs loaded on Cs-gel contributed to the diverse microstructure of the gel. The same phenomenon was observed in the other TPA parameters, including chewiness and gumminess. CCF-9 showed high texture and physical characteristics, including hardness, chewiness, and gumminess. Moreover, SEM micrographs indicated that the structure of the gel became more compact after binding Fs, resulting in strong TPA parameters (Zhong et al., 2022).

3.6. Cumulative release (%) of Fs from prepared gel and their binding mechanism

The release profiles of Fs from the CCF-3, CCF-5, CCF-7, and CCF-9 were measured by monitoring total concentration released at 720 min, as displayed in Fig. S2. Results revealed that the amount of Fs eluted from the prepared gel increased in the following order CCF-3 < CCF-5 < CCF-7 < CCF-9. The release of Fs reached 72.59 % for CCF-3, 75.49 % for CCF-5, 84.49 % for CCF-7, and 87.08 % for CCF-9. These results could be attributed to the higher hydrophilicity of CCF-9 triggered structural relaxation, resulting in a higher release of Fs. Phonrachom, Charoensuk,

Table 1
Texture profile analysis of Cs, CCN, CCF-3, CCF-5, CCF-7, and CCF-9.

Samples	Physical properties							Physical appearances
	Hardness (g)	Adhesiveness (g. sec)	Cohesiveness (%)	Resilience (%)	Springiness (%)	Chewiness	Gumminess	
Cs	93.76 ± 5.20 ^c	-84.69 ± 0.75 ^a	11.56 ± 0.53 ^a	1.22 ± 0.09 ^a	19.43 ± 0.50 ^a	210.47 ± 5.07 ^a	1083.46 ± 2.85 ^c	
CCN	78.42 ± 2.45 ^b	-68.61 ± 7.67 ^b	12.62 ± 0.96 ^{ab}	1.21 ± 0.01 ^a	23.72 ± 1.45 ^b	222.27 ± 2.57 ^b	908.80 ± 51.03 ^b	
CCF-3	55.29 ± 2.23 ^a	-28.56 ± 1.10 ^d	13.72 ± 0.94 ^{bc}	1.35 ± 0.05 ^b	31.64 ± 3.13 ^c	235.26 ± 4.92 ^c	791.75 ± 10.53 ^a	
CCF-5	82.26 ± 1.07 ^b	-87.07 ± 1.69 ^a	17.82 ± 0.66 ^e	1.26 ± 0.06 ^{ab}	47.69 ± 2.19 ^f	712.55 ± 1.85 ^d	1479.60 ± 5.46 ^d	
CCF-7	144.42 ± 2.39 ^d	-33.75 ± 1.65 ^{cd}	15.25 ± 1.53 ^{cd}	1.24 ± 0.05 ^a	38.82 ± 1.66 ^d	779.44 ± 1.02 ^e	2096.97 ± 7.59 ^e	
CCF-9	152.66 ± 3.18 ^e	-36.99 ± 2.50 ^e	16.19 ± 1.25 ^{de}	1.20 ± 0.02 ^a	43.51 ± 0.57 ^e	807.92 ± 6.49 ^f	2124.58 ± 3.72 ^e	

Values are the mean ± standard deviation of three replicates. Different letters in the same column indicate significant differences among the results ($p < 0.05$).

Kiti, Saichana, Kakumyan, and Suwanton (2023) reported that propolis loaded on chitosan/pectin hydrogel increased the hydrophilicity resulting in faster release of the propolis. Another explanation was reported by Athipornchai et al. (2024) indicating that the high amount of mangiferin loaded on carrageenan/chitosan hydrogel exhibited the highest cumulative release (%). All prepared gels exhibited a high cumulative release (%) at 180 min, followed by slower and sustained release rate till the end of the analysis.

The binding free energy ($\Delta G_{\text{binding}}$) and binding energy (ΔE) showed negative values, suggesting that the calculations at the M062X/6-31G (d, p) level of theory could provide a useful understanding of the binding among molecules inside the gel matrix and most importantly its stability during processing where this interaction was a spontaneous and exothermic. As portrayed in Fig. 9, Cs stacked with CN, where there are no direct binding forces among them occurred, where adding TPP directly conjugated between CN and Cs with a couple of H-bonds and some other π - π stacking interactions. Meanwhile, Pa could also directly interact with Cs by 2 H-bonds and other π - π forces since its delocalized electrons, leading to stabilizing the gel stability and agreeing with our characterization results. Narirutin, the key flavonoid fraction of our flavonoid extract, also interacts with Cs in the presence of Pa by H-bonding, showing the importance of the dual crosslinkers we used. The Surflex-dock results found that CCF final gel conjugates have an acceptable polarizability with a value of 1.031. In addition to the close contacts between the flavonoid and benzene rings of each ligand used and their equals Cs which may enhance their binding among the gel matrices, finally leading to stabilizing its functional and supplementary uses. It was speculated that H-bonding and π - π interactions of the gel ligands were the main driving forces of their stabilization. These forces mainly assisted the multiple

ligands in the presence of suitable crosslinkers to improve the gels stabilization and prevent their deterioration. PCA is a statistical analysis used to link all variables together. PCA data showed that the analysis of the first and second components (PC_1 and PC_2) were 57.21 and 23.71%, respectively, with a cumulative variation contribution ratio of 80.92% (more than 75–85%). PC_1 exhibited a positive correlation with all gel parameters including antioxidant ability, antifungal against *P. expansum* and *A. westerdijkiae*, antibacterial against *S. aureus*, *E. coli*, and *B. cereus*, and TPA (Fig. 10A). Moreover, PC_1 exhibited a positive correlation with CCF-5, CCF-7, and CCF-9 gels, displaying their preferred effecting on the tested parameters, while the Cs, CCN, and CCF-3 gels showed a positive correlation with PC_2 . These findings agreed with the experimental data, where the high amount of Fs (9 mg/mL) and CN (250 μ g/mL) were more significant effective than Cs-gel. Thereby, these data suggested that the integrated flavonoid with CCN gel have influenced the analyzed parameters. As revealed in Fig. 10B, the Pearson correlation analysis displayed that a great significant of $p < 0.001$ between (ABTS and DPPH), (*P. expansum* and *A. westerdijkiae*), (*S. aureus*, *E. coli*, and *B. cereus*), (all TPA parameters), indicating to a great effect on each other. There are different colors of bubbles Pearson correlation represented by red, blue, and so on. However, the most important is the high shadow color, which presents the high correlation and vice versa. Significantly, almost all the parameters exhibit a positive correlation, indicating a strong association among the selected gel variables used to assess the effects of CN and Fs on Cs-gel structure.

4. Conclusion

The ionic-gelation method successfully fabricated chitosan gel (Cs)

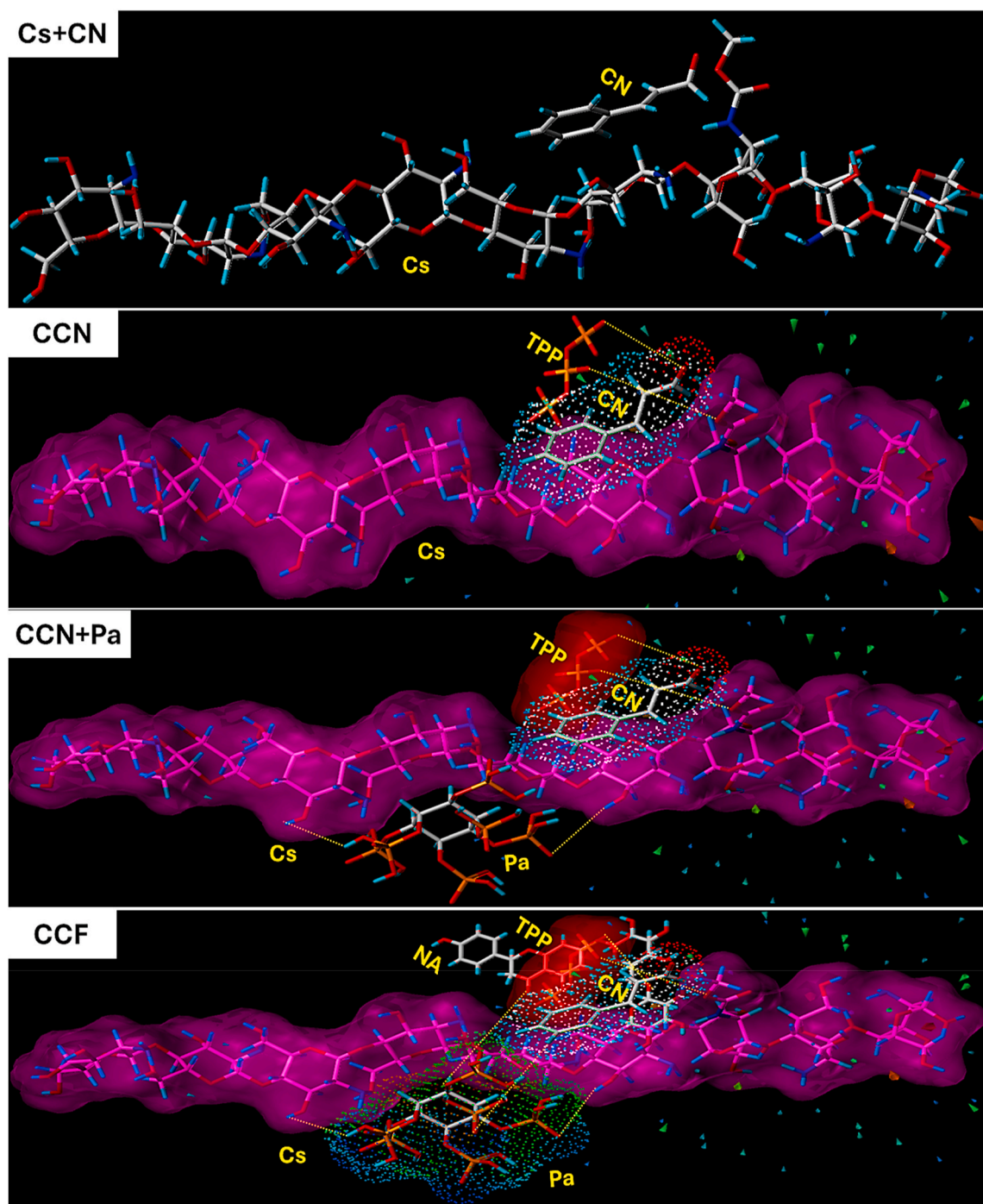


Fig. 9. The MD possibilities of the inter-intramolecular interaction among the gel formulas (Fs/CN/Cs) using triphosphate and phytic acid as cross-linkers, the double yellow dashed lines (—) referred to H-bonding among them, while from the pink to the red areas and small sticks referred to the suspected positions of the H-bonds, electrostatic, and hydrophobicity forces. (For interpretation of the references to color in this figure legend, the reader is referred to the Web version of this article.)

functionalized with cinnamaldehyde oil (CN) and flavonoid extract (Fs) and assessed their antioxidant and antimicrobial effects. The EE of CCF ranged from $75.95 \pm 1.74\%$ to $83.14 \pm 3.34\%$ based on an increase in flavonoid concentration, while the EE of CCN was at $80.56 \pm 1.17\%$. The UV and FTIR spectra revealed that H-bond formation in the original binary complex was the main force dominating the interaction, in accordance with XRD, Raman spectroscopy, and Surfex-dock findings. Furthermore, Cs-gel successfully encapsulated Fs and CN, as evidenced by XPS and SEM-EDX micrographs. The CCF-9 gels showed potential antioxidant levels of $38.22 \pm 0.37 \mu\text{g/mL}$ against DPPH free radicals and

$174.170 \pm 1.36 \mu\text{g/mL}$ against ABTS free radicals. The antifungal inhibitory activity (%) against *P. expansum* and *A. westerdijkiae* of CCF-9 was 29.91 ± 1.22 and $93.61 \pm 2.12\%$, respectively. In addition, CCF-9's zone growth inhibition effects against *S. aureus*, *E. coli*, and *B. cereus* were 28.65 ± 0.05 , 27.69 ± 0.04 , and 26.16 ± 0.02 mm, respectively. Texture properties revealed that the hardness and springiness increased in the order $\text{CCF-3} < \text{CCF-5} < \text{CCF-7} < \text{CCF-9}$, further accomplishing the cumulative release (%) findings. These results showed the potential antioxidant and antimicrobial effects of Cs-gel functionalized with cinnamaldehyde oil and flavonoid extract, suggesting it as a potential

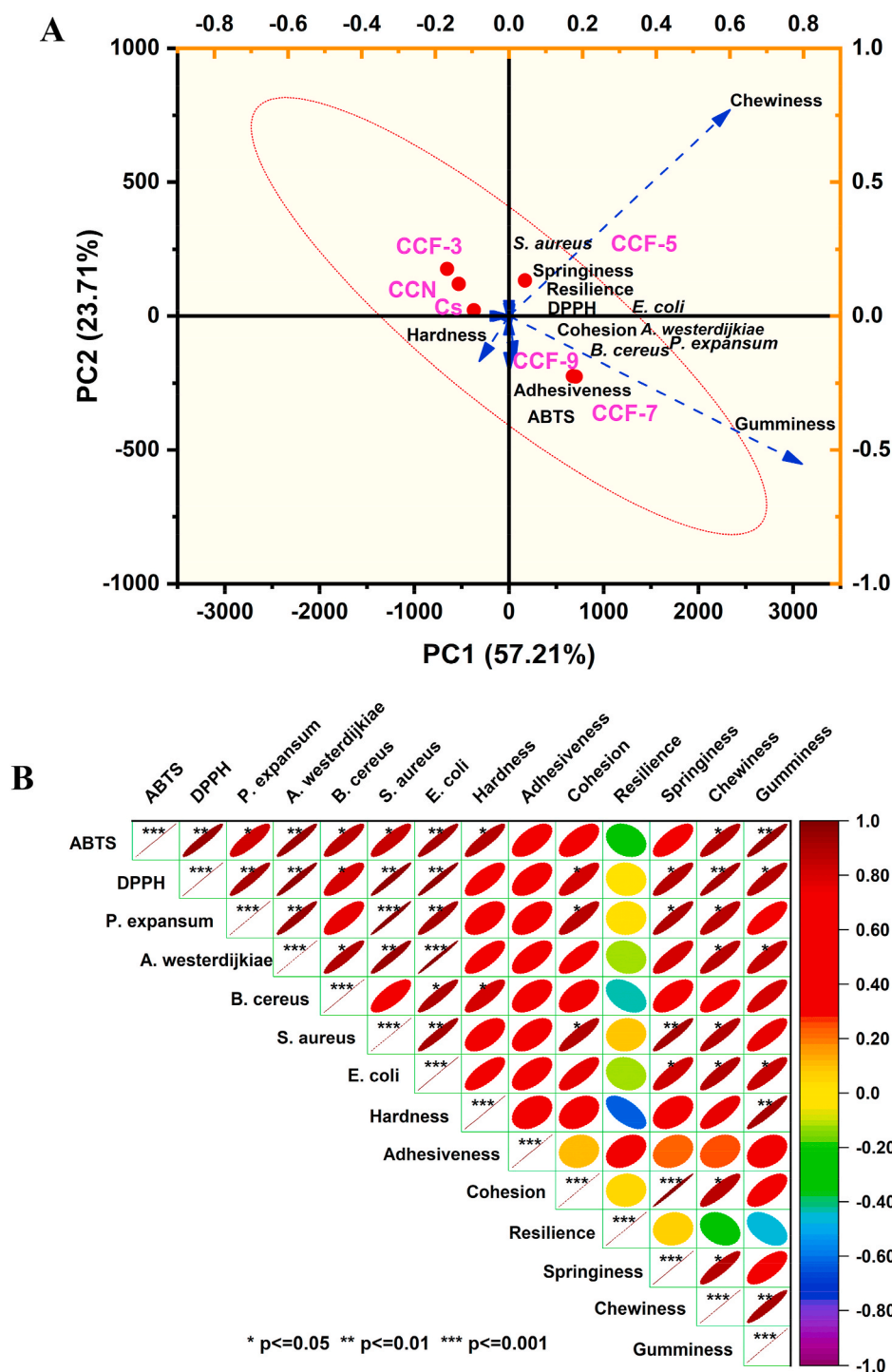


Fig. 10. Principle component analysis (A) and bubbles Pearson correlation analysis for the gels variables (B). *, **, and *** are the significant levels of 0.05, 0.01, and 0.001, respectively.

additive in the food or pharmaceutical industries.

CRediT authorship contribution statement

Mahmoud Salah: Conceptualization, Methodology, Investigation, Writing – original draft. **Juanying Huang:** Data curation. **Chenyang Zhu:** Validation. **Mabrouk Sobhy:** Writing – review & editing. **Mohamed A. Farag:** Writing – review & editing. **Yajing Fang:** Software, Visualization. **Remah Sobhy:** Visualization, Writing – review & editing. **Noman Walayat:** Software, Visualization. **Ibrahim Khalifa:**

Data curation. **Sajid Maqsood:** Supervision, Resources, Writing: Revision, editing and proof reading. **Yun Wang:** Supervision, Resources.

Declaration of competing interest

No conflict of interest among authors.

Data availability

Data will be made available on request.

Acknowledgments

This work was partially supported by the National Natural Science Foundation of China (32072639). The authors are also would like to thank United Arab Emirates University for their post-doc fund (12F047) under climatic action research theme.

Appendix A. Supplementary data

Supplementary data to this article can be found online at <https://doi.org/10.1016/j.crfs.2024.100826>.

References

- Adame, M.Y., Shi, C., Li, C., Aziz, T., Alharbi, M., Cui, H., Lin, L., 2024. Fabrication and characterization of pullulan/tapioca starch-based antibacterial films incorporated with Litsea cubeba essential oil for meat preservation. *Int. J. Biol. Macromol.* 268, 131775.
- Addi, M., Elbouzidi, A., Abid, M., Tungmunthum, D., Elamrani, A., Hano, C., 2021. An overview of bioactive flavonoids from citrus fruits. *Appl. Sci.* 12 (1), 29.
- Aluani, D., Tzankova, V., Yordanov, Y., Kondeva-Burdina, M., Yoncheva, K., 2017. In vitro protective effects of encapsulated quercetin in neuronal models of oxidative stress injury. *Biotechnol. Biotechnol. Equip.* 31 (5), 1055–1063.
- Arya, S.S., Rookes, J.E., Cahill, D.M., Lenka, S.K., 2022. Chitosan nanoparticles and their combination with methyl jasmonate for the elicitation of phenolics and flavonoids in plant cell suspension cultures. *Int. J. Biol. Macromol.* 214, 632–641.
- Athipornchai, A., Pabunrueang, P., Trakulsujaritchook, T., 2024. Mangiferin loaded carrageenan/chitosan core-shell hydrogel beads: preparation, characterization and proposed application. *Food Hydrocolloids* 147, 109394.
- Chen, C., Li, Z., Wang, C., Liu, S., Wang, Y., Zhang, M., Tian, Y., Lv, J., Xu, H., Xia, G., 2023. Stability and antioxidant activity of chitosan/ β -Lactoglobulin on anthocyanins from *Aronia melanocarpa*. *Lebensm. Wiss. Technol.* 173, 114335.
- Chen, H., Hu, X., Chen, E., Wu, S., McClements, D.J., Liu, S., Li, B., Li, Y., 2016. Preparation, characterization, and properties of chitosan films with cinnamaldehyde nanoemulsions. *Food Hydrocolloids* 61, 662–671.
- Ciobanu, S.C., Predoi, D., Chifriuc, M.C., Iconaru, S.L., Predoi, M.V., Popa, M., Rokosz, K., Raaen, S., Marinas, I.C., 2023. *Salvia officinalis*-hydroxyapatite nanocomposites with antibacterial properties. *Polymers* 15 (23), 4484.
- Coutinho, T.C., Ferreira, M.C., Rosa, L.H., de Oliveira, A.M., Oliveira Júnior, E.N.d., 2020. *Penicillium citrinum* and *Penicillium mallochii*: new phytopathogens of orange fruit and their control using chitosan. *Carbohydr. Polym.* 234, 115918.
- Cox, H., Li, J., Saini, P., Paterson, J., Sharples, G., Badyal, J., 2021. Bioinspired and eco-friendly high efficacy cinnamaldehyde antibacterial surfaces. *J. Mater. Chem. B* 9.
- Ding, Z., Mo, M., Zhang, K., Bi, Y., Kong, F., 2021. Preparation, characterization and biological activity of proanthocyanidin-chitosan nanoparticles. *Int. J. Biol. Macromol.* 188, 43–51.
- Do, N.H.N., Truong, Q.T., Le, P.K., Ha, A.C., 2022. Recent developments in chitosan hydrogels carrying natural bioactive compounds. *Carbohydr. Polym.* 294, 119726.
- Doyle, A.A., Stephens, J.C., 2019. A review of cinnamaldehyde and its derivatives as antibacterial agents. *Fitoterapia* 139, 104405.
- Duan, Y., 2014. In: *Ultraviolet-Visible Spectrum Characterizations of Quercetin in Aqueous Ethanol Solution with Different pH Values*.
- García, M.V., Brêgão, A.S., Parussolo, G., Bernardi, A.O., Stefanello, A., Copetti, M.V., 2019. Incidence of spoilage fungi in the air of bakeries with different hygienic status. *Int. J. Food Microbiol.* 290, 254–261.
- Gong, W., Sun, Y., Tu, T., Huang, J., Zhu, C., Zhang, J., Salah, M., Zhao, L., Xia, X., Wang, Y., 2024. Chitosan inhibits *Penicillium expansum* possibly by binding to DNA and triggering apoptosis. *Int. J. Biol. Macromol.* 259, 129113.
- Guo, L., Li, Y., Mao, X., Tao, R., Tao, B., Zhou, Z., 2022. Antifungal activity of polymethoxylated flavonoids (PMFs)-Loaded citral nanoemulsion against *Penicillium italicum* by causing cell membrane damage. *Journal of Fungi* 8 (4), 388.
- Hernández, A., Ruiz-Moyano, S., Galván, A.I., Merchán, A.V., Pérez Nevado, F., Aranda, E., Serradilla, M.J., Córdoba, M.d.G., Martín, A., 2021. Anti-fungal activity of phenolic sweet orange peel extract for controlling fungi responsible for post-harvest fruit decay. *Fungal Biol.* 125 (2), 143–152.
- Jha, R., Mayanovic, R.A., 2023. A review of the preparation, characterization, and applications of chitosan nanoparticles in nanomedicine. *Nanomaterials* 13 (8).
- Jiang, F., Duan, Y., Li, Q., Li, X., Li, Y., Wang, Y., Liu, S., Liu, M., Zhang, C., Pan, X., 2024. Insect chitosan/pullulan/gallium photo-crosslinking hydrogels with multiple bioactivities promote MRSA-infected wound healing. *Carbohydr. Polym.* 334, 122045.
- Khalifa, I., Du, J., Nawaz, A., Li, C., Agriculture, 2021. Multiple co-pigments of quercetin and chlorogenic acid blends intensify the color of mulberry anthocyanins: insights from hyperchromicity, kinetics, and molecular modeling investigations, 101 (4), 1579–1588.
- Khorshidi, S., Khoobakht, F., Mirmoghtadaie, L., Hosseini, S.M., 2023. Characterization of gellan gum-chitosan based hydrogel to evaluate as a potential gelatin substitute. *Food Hydrocolloids* 145, 109038.
- Lai, C., Huang, M., Xiong, Q., Liang, Y., Jiang, Y., Zhang, J., 2024. Green and efficient approach to extract bioactive flavonoids with antioxidant, antibacterial, antiglycation, and enzyme inhibitory activities from navel orange peel. *Sustain. Chem. Pharm.* 38, 101479.
- Li, F., Jin, H., Xiao, J., Yin, X., Liu, X., Li, D., Huang, Q., 2018. The simultaneous loading of catechin and quercetin on chitosan-based nanoparticles as effective antioxidant and antibacterial agent. *Food Res. Int.* 111, 351–360.
- Li, J., Jiang, Q., Sun, L., Zhang, J., Han, Z., Xu, S., Cheng, Z., 2024. Adsorption of heavy metals and antibacterial activity of silicon-doped chitosan composite microspheres loaded with ZIF-8. *Separ. Purif. Technol.* 328, 124969.
- Liang, Q., Sun, X., Raza, H., Aslam Khan, M., Ma, H., Ren, X., 2021. Fabrication and characterization of quercetin loaded casein phosphopeptides-chitosan composite nanoparticles by ultrasound treatment: factor optimization, formation mechanism, physicochemical stability and antioxidant activity. *Ultrason. Sonochem.* 80, 105830.
- Liu, Q., Cui, H., Muhoza, B., Duhoranimana, E., Xia, S., Hayat, K., Hussain, S., Tahir, M. U., Zhang, X., 2020. Fabrication of low environment-sensitive nanoparticles for cinnamaldehyde encapsulation by heat-induced gelation method. *Food Hydrocolloids* 105, 105789.
- Liu, Y., Benohoud, M., Galani Yamdeu, J.H., Gong, Y.Y., Orfila, C., 2021. Green extraction of polyphenols from citrus peel by-products and their antifungal activity against *Aspergillus flavus*. *Food Chem.* X 12, 100144.
- Nalini, T., Basha, S.K., Sadiq, A.M., Kumari, V.S., 2022. In vitro cytocompatibility assessment and antibacterial effects of quercetin encapsulated alginate/chitosan nanoparticle. *Int. J. Biol. Macromol.* 219, 304–311.
- Pereira Silveira, M., Lucas Chaves Almeida, F., Dutra Alvim, I., Silvia Prata, A., 2023. Encapsulation of pomegranate polyphenols by ionic gelation: strategies for improved retention and controlled release. *Food Res. Int.* 174, 113590.
- Phonrachom, O., Charoensuk, P., Kiti, K., Saichana, N., Kakumyan, P., Suwanton, O., 2023. Potential use of propolis-loaded quaternized chitosan/pectin hydrogel films as wound dressings: preparation, characterization, antibacterial evaluation, and in vitro healing assay. *Int. J. Biol. Macromol.* 241, 124633.
- Predoi, D., Iconaru, S.L., Buton, N., Badea, M.L., Marutescu, L., 2018. Antimicrobial activity of new materials based on lavender and basil essential oils and hydroxyapatite. *Nanomaterials* 8 (5), 291.
- Predoi, D., Iconaru, S.L., Ciobanu, C.S., Raita, M.S., Ghegoiu, L., Trusca, R., Badea, M.L., Cimpeanu, C., 2023. Studies of the tarragon essential oil effects on the characteristics of doped hydroxyapatite/chitosan biocomposites. *Polymers* 15 (8), 1908.
- Ren, J., Tong, J., Li, P., Huang, X., Dong, P., Ren, M., 2021. Chitosan is an effective inhibitor against potato dry rot caused by *Fusarium oxysporum*. *Physiol. Mol. Plant Pathol.* 113, 101601.
- Roy, P., Parveen, S., Ghosh, P., Ghatak, K., Dasgupta, S., 2019. Flavonoid loaded nanoparticles as an effective measure to combat oxidative stress in Ribonuclease A. *Biochimie* 162, 185–197.
- Salah, M., Mansour, M., Zogona, D., Xu, X., 2020. Nanoencapsulation of anthocyanins-loaded β -lactoglobulin nanoparticles: characterization, stability, and bioavailability in vitro. *Food Res. Int.* 137, 109635.
- Salah, M., Xu, X., 2021. Anthocyanin- β -lactoglobulin nanoparticles in acidic media: synthesis, characterization and interaction study. *J. Mol. Struct.* 1232, 129995.
- Subhaswaraj, P., Barik, S., Macha, C., Chiranjeevi, P.V., Siddhardha, B., 2018. Anti quorum sensing and anti biofilm efficacy of cinnamaldehyde encapsulated chitosan nanoparticles against *Pseudomonas aeruginosa* PAO1. *Lebensm. Wiss. Technol.* 97, 752–759.
- Sun, J., Chen, J., Mei, Z., Luo, Z., Ding, L., Jiang, X., Bai, W., 2020. Synthesis, structural characterization, and evaluation of cyanidin-3-O-glucoside-loaded chitosan nanoparticles. *Food Chem.* 330, 127239.
- Thebti, A., Meddeb, A., Ben Salem, I., Bakary, C., Ayari, S., Rezgui, F., Essafi-Benkhadir, K., Boudabous, A., Ouzari, H.L., 2023. Antimicrobial activities and mode of flavonoid actions. *Antibiotics (Basel)* 12 (2).
- Tu, T., Ren, Y., Gong, W., Huang, J., Zhu, C., Salah, M., Zhao, L., Xia, X., Wang, Y., 2024. Endoglucanase H from *Aspergillus westerdijkiae* plays an important role in the virulence on pear fruits. *J. Agric. Food Chem.* 72 (15), 8415–8422.
- Wang, L., Xin, M., Li, M., Liu, W., Mao, Y., 2023. Effect of the structure of chitosan quaternary phosphonium salt and chitosan quaternary ammonium salt on the antibacterial and antibiofilm activity. *Int. J. Biol. Macromol.* 242, 124877.
- Wu, Y., Gao, H., Liu, J., Liang, H., 2023. Chitosan nanoparticles efficiently enhance the dispersibility, stability and selective antibacterial activity of insoluble isoflavonoids. *Int. J. Biol. Macromol.* 232, 123420.
- Zhang, J., Zhang, L., Lai, C., Liang, Y., Gao, L., Kaliaperumal, K., Jiang, Y., 2022. Nutraceutical potential of navel orange peel in diabetes management: the chemical profile, antioxidant, α -glucosidase inhibitory and antiglycation effects of its flavonoids. *Food Biosci.* 49, 101943.
- Zhang, Y., Yang, Y., Tang, K., Hu, X., Zou, G., 2008. Physicochemical characterization and antioxidant activity of quercetin-loaded chitosan nanoparticles. *J. Appl. Polym. Sci.* 107 (2), 891–897.
- Zhong, Y., Yang, L., Dai, T., Zhu, Z., Chen, H., Wu, J., Gong, E.S., 2022a. Flavonoids enhance gel strength of ovalbumin: properties, structures, and interactions. *Food Chem.* 387, 132892.
- Zhong, Y., Yang, L., Zhu, Z., Chen, H., Liu, C., Dai, T., Gong, E.S., 2022b. Protective effect of ovalbumin-flavonoid hydrogel on thrombolytic activity and stability of nattokinase. *Food Res. Int.* 156, 111188.
- Zhou, H.Y., Hao, P.Y., Jiang, S.Q., Zhang, W.H., Ren, L.J., Zheng, H.J., Chen, Y.W., Chen, J.L., Park, H.J., 2024. Preparation and antibacterial activity of chitosan grafted cyclodextrin hydrogel loaded berberine hydrochloride using dual gelling agent. *J. Mol. Struct.* 1295, 136709.